First Comparative Analysis of Simulated Low and High Resolution Hydroterra and Conventional SAR Data

Jens Fischer[a], Rolf Scheiber[a], Ralf Horn[a], and Julia Kubanek[b]
[a]German Aerospace Center (DLR), Microwaves and Radar Institute, Wessling, Germany
[b]European Space Agency (ESA), ESTEC, Noordwijk, The Netherlands

Abstract

Hydroterra was a mission proposal considered as one of three concepts for ESA's Earth Explorer 10 mission. Its concept is to place a Synthetic Aperture Radar (SAR) into a geosynchronous orbit to measure key processes of the diurnal water cycle over regions in Europe and Africa. The azimuth integration time is thereby substantially longer compared to conventional SAR systems and it is important to know to what extent this influences the retrieval of (i) snow water equivalent (SWE) and (ii) surface soil moisture (SSM) estimates extracted from these data. To study these effects, the DLR Microwaves and Radar Institute conducted airborne SAR campaigns, 2019 at Kaufbeuren (Germany), 2021 at Wörgetal (Austria) and 2022 at Foggia (Italy). In this paper, we compare simulated Hydroterra (long integration) and conventional (short integration) SAR data acquired at Foggia. We analyze (i) image amplitude, (ii) image contrast and (iii) interferogram (coherency and phase) degradations due to temporal decorrelation on different vegetation periods (April and June) in low (Hydroterra specification) and in high (airborne SAR) resolution data, respectively.

1 Introduction

The Hydroterra mission, formerly Geosynchroneous Continental Land-Atmosphere Sensing System (G-CLASS) [1][2], was one of the three mission candidates (Daedalus, Hydroterra, Harmony) for the European Space Agency's 10th Earth Explorer mission and recently ESA decided to move on to the next phase of development with Harmony [3]. The Hydroterra concept was to place a Synthetic Aperture Radar (SAR) system into a geosynchronous orbit to enable continuous monitoring of selected areas of interest over Europe and Africa. The mission focus is to monitor the diurnal water cycle which includes, amongst others, the retrieval of atmospheric water vapor, snow water equivalent (SWE) and surface soil moisture (SSM) estimates. The main characteristics of a geosynchronous SAR system is that long azimuth integration times arise which are required to generate image products with an azimuth resolution comparable to those obtained from low-Earth orbit (LEO) SAR missions. Long integration times, on the other hand, introduce temporal decorrelation and therefore studies are needed to investigate the effect of temporal decorrelation on Hydroterra data compared to conventional SAR data. The German Aerospace Center (DLR) Microwaves and Radar Institute (HR) conducted several airborne campaigns towards this goal using F-SAR, their airborne multi-frequency (P-, L-, S-, C-, X-band) fully polarimetric SAR system mounted on a Do-228 Dornier aircraft [4]. A first experiment took place 2019 at Kaufbeuren (Germany) [5][6][7], another one, dedicated to the retrieval of snow water equivalent (SWE), took place 2021 at Wörgetal [8][9][10] (Austria) and the latest one, dedicated to the retrieval of surface soil moisture (SSM) took place 2022 at Foggia, Italy. This paper reports on the analysis of simulated Hydroterra data, generated from F-SAR data, which were acquired 2022 at Foggia for the purposes of investigating the effect of temporal decorrelation on the retrieval of surface soil moisture (SSM) estimates. Foggia with its many different agricultural areas is a site that is under intensive observation for research purposes by the Consiglio Nazionale delle Richerche (CNR), Instituto per il Rilevamento Elettromagnetico dell'Ambiente (IREA). In this paper, we focus on the analysis of Single Look Complex (SLC) image and interferogram quality degradations due to temporal decorrelation. For that, it turned out to be helpful to have knowledge about crop types in the fields. We do not investigate impacts on the soil moisture retrieval in this paper, it will be done in a follow-on study. In Section 2, we describe the airborne SAR campaign near Foggia and the simulation data we created, Section 3 describes quality measures we use and in Section 4 we present first results, the most important outcomes so far, on the comparison of simulated Hydroterra SAR data compared to conventional SAR data.

2 Foggia Airborne Campaign

The F-SAR campaign at Foggia, southern Italy, took place from 28-29 April 2022 (mission 01) and from 15-16 June 2022 (mission 02). In this way, we acquired data on different vegetation periods. One of the goals is to investigate whether the crop height has an influence on the strength of the observed temporal decorrelation effects. We acquired data in C- and L-band, simultaneously. C-band is the band intended for the realization of Hydroterra and L-band data

have been recorded for comparison in support of the upcoming ROSE-L mission. In this paper, we only report on C-band results (simulated Hydroterra data). Using F-SAR, DLR's airborne SAR, we acquired C-band data with 384 MHz bandwidth at 5.3 GHz center frequency. Every day (28-29 April, 15-16 June), we had a morning and an afternoon flight. The first three flights in each mission included approximately 12 repetitions (passes) per flight, imaging the same scenery (spatial extent) but with temporal baselines of approximately ten minutes. They are used to create simulated Hydroterra products.

2.1 Hydroterra Products

The first three flights in each mission (April: FL01, FL02, FL03 and June: FL05, FL06, FL07) are dedicated to Hydroterra. We created six simulated Hydroterra products from these flights according to the ESA scenario 4 requirement [11][12] which is given in **Table 1**.

Table 1 Hydroterra Product (scenario 4).

Parameter	Value
SLC azimuth resolution	5 m
ML azimuth resolution	50 m
Number of looks in azimuth	10
Range bandwidth	6 MHz
SLC slant range resolution	22.2 m
ML slant range resolution	22.2 m
Number of looks in range	1
Noise Equivalent Sigma Zero	-21.1 dB

Long azimuth times are simulated by coherently joining the individual bandwidths of up to 12 passes in each flight (see [5][6][7] for details), the resulting products are listed in **Table 2**.

Table 2 Simulated Images & Interferograms.

Mission	Product	Hydroterra	Conventional
April	SLC 01	FL01	0104
April	SLC 02	FL02	0204
April	SLC 03	FL03	0304
June	SLC 05	FL05	0504
June	SLC 06	FL06	0604
June	SLC 07	FL07	0704
April	IF 01	FL01-FL02	0104-0204
April	IF 02	FL02-FL03	0204-0304
April	IF 03	FL01-FL03	0104-0304
June	IF 05	FL05-FL06	0504-0604
June	IF 06	FL06-FL07	0604-0704
June	IF 07	FL05-FL07	0504-0704

The technique used to fuse image bandwidths (in azimuth) of individually acquired passes coherently (same spatial scene at different times) is the one used in *distributed imaging* [13,14].

The respective conventional SAR products to which we compare Hydroterra products are created from only one pass in each flight, the first one (pass 04). We refer to these conventional SAR image products as 0104, 0204, 0304 (in April) and 0504, 0604, 0704 (in June), see **Table 2**. The quality of conventional SAR data, acquired by F-SAR, is given in **Table 3**, right column, where the NESZ varies as a function of off-nadir angle.

Table 3 SLC Data Quality.

Resolution	Hydroterra	Conventional
Azimuth	5 m	0.5 m
Slant Range	22 m	0.5 m
NESZ	-21 dB	-25 to -40 dB

Furthermore, we created interferograms of these images, see **Table 2**. Three images per mission (April and June) allowed to form three interferograms per mission. Interferograms allow us to investigate the impact of long azimuth integration times on the observation of irrigation on fields, for example. See the results below (Section 4.3).

2.2 Integration Time vs. Resolution

Hydroterra SAR compared to conventional SAR data are characterized by two important differences, i.e., (i) long versus short azimuth integration times (**Table 4**, on conventional SAR data we have 2.5 sec in near and 4.6 sec in far range) and (ii) low versus high resolution (**Table 3**, on conventional SAR data we have 0.5 m in azimuth and 0.5 m in slant range). In order study these effects separately, we created an intermediate product, called GEO-SAR (geosynchronous SAR satellite system), with -21 dB NESZ, Hydroterra SAR azimuth integration time and F-SAR resolution. We refer to it as GEO (high resolution) compared to HT (low resolution), the Hydroterra SAR satellite.

Table 4 Long vs. Short Azimuth Integration Times.

Pass	Hydroterra	Conventional
FL01	119.05 min	2.5 - 4.6 sec
FL02	113.70 min	2.5 - 4.6 sec
FL03	115.15 min	2.5 - 4.6 sec
FL05	112.36 min	2.5 - 4.6 sec
FL06	109.62 min	2.5 - 4.6 sec
FL07	113.64 min	2.5 - 4.6 sec

The two data qualities, GEO and HT (Hydroterra SAR), compared to F-SAR data allow us to study the effect of short and long azimuth integration times, decoupled from resolution. It turns out that the effect of long azimuth integration times leads to a noticeable quality loss in GEO data compared to F-SAR data but this loss can barely be observed in HT data due to its low resolution, as will be described in Section 4.

3 Quality Measures

In order to compare Hydroterra SAR, GEO-SAR and F-SAR data on single-look-complex (SLC) images and interferograms we studied the degradation of (i) image amplitudes, (ii) image contrasts and (ii) interferogram coherencies, respectively. Image mean values are calculated by the formula

$$\mu_{\text{dB}} = 10\ \log_{10}(\ \mathbb{E}(I^2)\ )$$

where $\mathbb{E}$ is the expectation value (mean) on the image intensity I^2 and I is the single-look complex image. The contrast is defined to be the coefficient of variation of the image intensity, i.e. the ratio between the standard deviation σ and the mean μ of the image intensity [15,16]

$$C = \frac{\sqrt{\mathbb{E}[(I^2 - \mathbb{E}(I^2))^2]}}{\mathbb{E}(I^2)} = \frac{\sigma}{\mu}$$

where $\sigma = \sqrt{\mathbb{E}[(I^2 - \mathbb{E}(I^2))^2]} = \sqrt{Var(I^2)}$ is the standard deviation and $\mu = \mathbb{E}(I^2)$ the mean value of the image intensity. Contrast is a measure to assess the focusing quality in images [15,16]. We calculate contrast values blockwise using a sliding window, image blocks are normalized with respect to their maximum value $I = I/max(I)$ prior to contrast calculation and the block size is chosen with respect to the image resolution. This adaption is required because pixels in high-resolution data (GEO) are square-shaped (0.5 m x 0.5 m) and those in low-resolution data (HT) are non-squared (5 m x 22.2 m). We used a block size of 16x16 pixels in high-resolution data and a block size of 32x8 pixels in low-resolution data. Furthermore, the coherency between two SLC images is the absolute value

$$\gamma = \frac{|\ \mathbb{E}(I_1\ I_2^*)|}{\sqrt{\mathbb{E}(I_1^2)\ \mathbb{E}(I_2^2)}}$$

of the normalized interferogram of image I_1 and I_2, the symbol $*$ indicates complex conjugation. We either measure amplitude, contrast or coherency degradations on entire images or on individual fields–whose crops are known. It required to geocode all images, i.e., the slant range geometry is converted to geo-referenced data which allowed us to cut-out fields using their bounding polygons.

4 Simulation Data Analysis

We present results using the three quality measures (i) image amplitude (ii) image contrast and (iii) interferogram coherency. Due to the many possibilities to compare short vs. long integration integration times: 3 measures, 2 missions (April vs. June), 2 resolutions (GEO vs. HT), 4 polarizations (HH, HV, VV, VH), 50 fields (different crop types) we only present most important results in this paper.

4.1 Impact on Image Contrast

A loss of the focusing quality in Hydroterra data is expected due to the long azimuth integration time for all objects that move in any way, e.g., vegetation at windy conditions: the longer the vegetation the more sensible to wind. This can indeed be observed in our simulated data. First of all, we have a look at the entire scene and later we look at individual fields. The entire scene is depicted in **Fig. 1** for high-resolution data (GEO) and in **Fig. 2** for low-resolution data (HT), long integration times on the right.

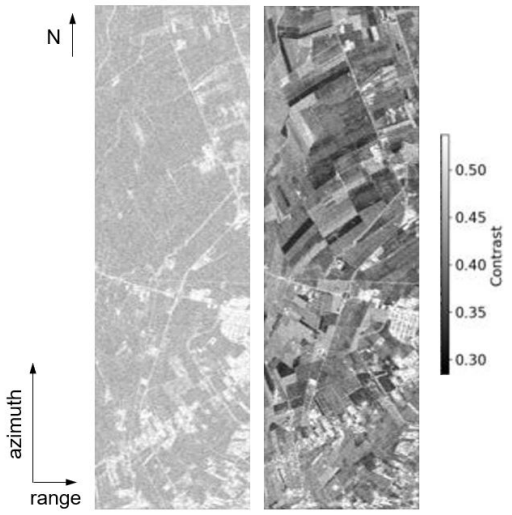

Figure 1 Image contrast (0104 vs. FL01), short integration (left) versus long integration (right) on high-resolution data (GEO), drops from **0.48** to **0.43**.

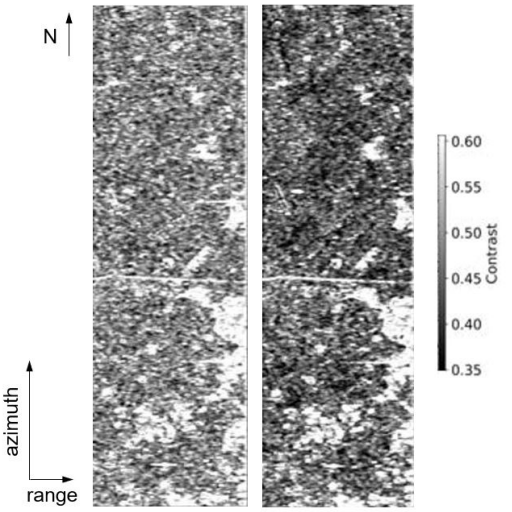

Figure 2 Image contrast (0104 vs. FL01), short integration (left) versus long integration (right) on low-resolution data (HT), drops from **0.51** to **0.48**.

In high-resolution data (GEO), we observe a drop in the overall contrast from 0.48 to 0.43, by 0.05, and in low-resolution data (HT), this drop is from 0.51 to 0.48, by merely 0.03. The start values 0.48 and 0.51 differ because different sliding window sizes had to be used (see Section 3). The trend observed here is typical for (simulated) Hydroterra data. Let us now have a look at individual fields, see our C-band, high-resolution F-SAR image, taken in April, in **Fig. 3** as an overview. Four example fields (horse bean, asparagus, tomato, maize) behave as shown in **Fig. 4** and **Fig. 5**. It is typical for the image degradations being studied on simulated Hydroterra data.

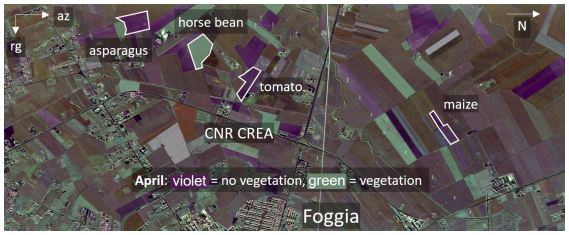

Figure 3 High-resolution F-SAR C-band image, taken in April (RGB=HH,HV,VV). Crops at the CNR CREA site, Foggia, see **Fig. 4** and **Fig. 5** below for their behavior.

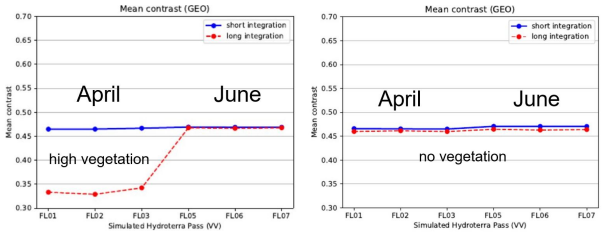

Figure 4 Mean image contrast on a *horse bean* field (left) versus an *asparagus* field (right), from April to June, GEO-SAR (VV). Other polarizations look similar.

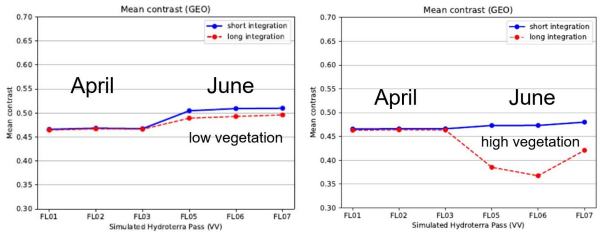

Figure 5 Mean image contrast on a *tomato* field (left) versus a *maize* field (right), from April to June, GEO-SAR (VV). Other polarizations look similar.

Because this is a typical behavior we observed, the conclusion can be drawn that image degradations (defocusing) occur with crop heights due to the sensitivity to wind.

4.2 Impact on Image Amplitudes

Image amplitudes are almost unaffected by the length of azimuth integration times and this applies to high-resolution (GEO) and low-resolution (HT) data likewise. It can be observed in **Fig. 6**, for example, where the blue and red curve do not differ considerably. The diagrams show mean amplitude values for field "CREA-BS", depicted in **Fig. 7** (GEO) and **Fig. 8** (HT) from April (FL01, FL02, FL03) to June (FL05, FL06, FL07). This field is under intensive observation by CNR, CREA. One studies, amongst others, the influence of drip irrigation (see Section 4.3.2) on this field. It can be seen (**Fig. 6**) that differences in mean image amplitude values between short (blue) and long (red) integrations are barely noticeable. The blue and the red curve are nearly identical. If the resolution of the image is not adequate, as can be seen in **Fig. 8**, then the effect of resolution surpasses the defocusing effect.
The field "CREA-BS" is obviously too small to allow monitoring the field variability in Hydroterra data (scenario 4).

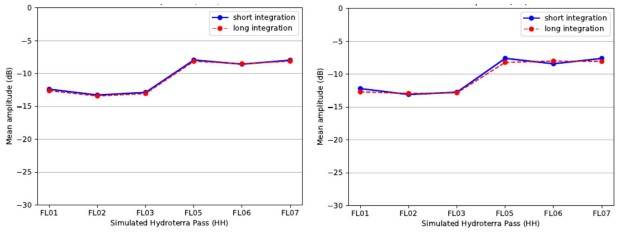

Figure 6 Mean amplitudes (HH) of FL01-FL07 in high (GEO, left) and low resolution (HT, right) data.

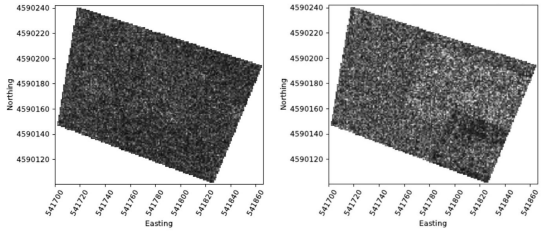

Figure 7 Amplitude image (HH) of FL01 (April, left) vs. FL05 (June, right) in high resolution (GEO-SAR). Their mean values are shown as red dots in **Fig. 6** (left).

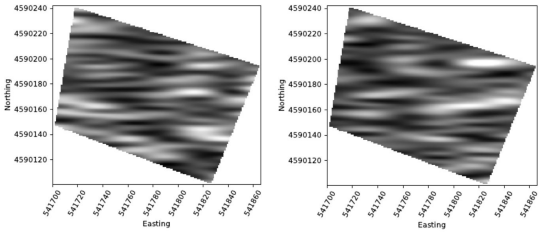

Figure 8 Amplitude image (HH) of FL01 (April, left) vs. FL05 (June, right) in low resolution (HT-SAR). Their mean values are shown as red dots in **Fig. 6** (right).

Its size of about 120 m by 80 m (see the UTM coordinates in **Fig. 8**, grid size given in 20 m steps) is not large enough to obtain reliable data. One may recall (**Table 1**), data in HT quality are resolved 5 [m] by 22.2 [m] in azimuth and range, respectively.

4.3 Impact on Interferograms

In this section, we study the impact of long azimuth integration times on the formation of interferograms.

4.3.1 Strip Irrigation

F-SAR flights (April mission) took place on April 28 and 29, 2022 and strip irrigation activities on monitored fields took place from April 23 to 29, 2022, i.e., such activities should be visible in interferograms from one flight (FL01, April 28 morning) to another (FL02, April 28 afternoon) and from one day (FL01, April 28 morning) to another (FL03, April 29 morning). Indeed, **Fig. 9** shows the irrigation activities (dark) in all three interferograms (left column), In contrast, there were no (known) irrigation activities (during the data takes) in June (right column). The mean values of all six images form the red curve in **Fig. 10** (left). We do not show short-integration images

(blue curve) as they look very similar (see **Fig. 10**) to those in **Fig. 9**. In general, it turns out that interferograms are almost unaffected by long azimuth integrations

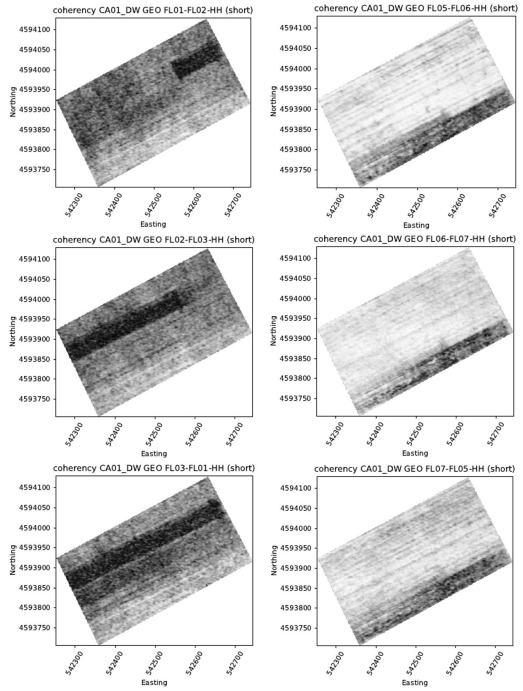

Figure 9 Coherency (HH) on field "CA01-DW", Durum wheat with strip irrigation, FL01-FL02, FL02-FL03, FL03-FL01 on the left (April) and FL05-FL06, FL06-FL07, FL07-FL05 on the right (June), on GEO data.

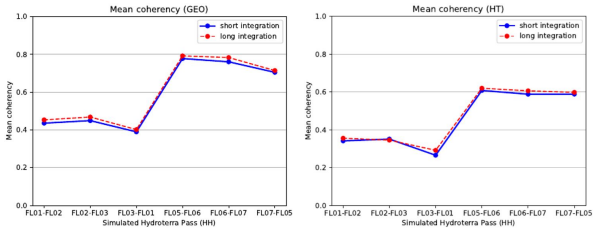

Figure 10 Mean coherency (HH), field "CA01-DW" with strip irrigation, high (GEO) vs. low (HT) resolution. The red curve corresponds to the six images in **Fig. 9**.

except for a very small coherency increase (see **Fig. 10**) which can be explained by the smoothing effect due to a defocusing in the images used to form the interferogram.

4.3.2 Drip Irrigation

We also investigated interferograms formed from data in which we strive to detect drip irrigation activities on selected fields. Drip irrigation activities took place from April 26 to 29, 2022, on field "CREA-BS". **Fig. 11** shows some of these activities and its turns out that, as above, long azimuth integration times have no significant influence on the formation of interferograms (**Fig. 12**). In contrast to this, resolution is important. As mentioned above (Section 4.2), field "CREA-BS" is too small to monitor field variability in simulated Hydroterra data (scenario 4), i.e., the values in **Fig. 12** (right) are not representative. As a result of that, the diagrams on the left and on the right in **Fig. 12** differ considerably.

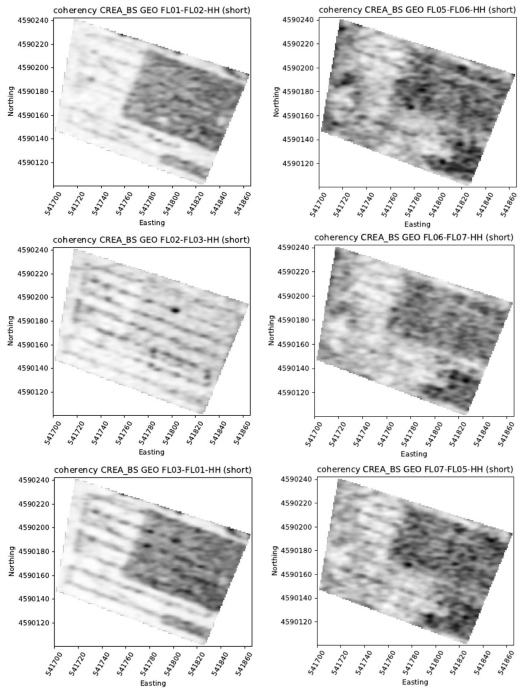

Figure 11 Coherency (HH) on field "CREA-BS", bare soil drip irrigation, FL01-FL02, FL02-FL03, FL03-FL01 on the left (April) and FL05-FL06, FL06-FL07, FL07-FL05 on the right (June), on GEO data.

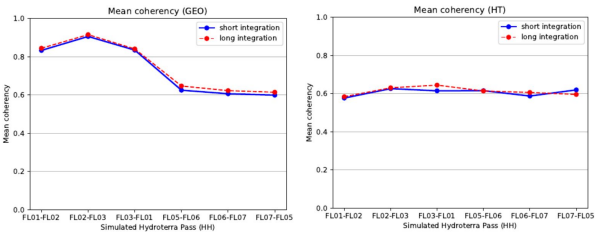

Figure 12 Mean coherency (HH), field "CREA-BS" with drip irrigation, high (GEO) vs. low (HT) resolution. The red curve corresponds to the six images in **Fig. 11**.

In contrast, field "CA01-DW" is of sufficient size (see **Fig. 9** (right), grid size given in 100 m steps), hence, the results given in Hydroterra quality, appear to be similar to those of high-resolution data, **Fig. 10** (left vs. right).

5 Conclusions

We investigated simulated Hydroterra SAR data to clarify the question of how great the influence of long azimuth integration times is compared to data acquired with conventional SAR systems with much shorter azimuth integration times. To decouple the effects of (i) long azimuth integration times and (ii) poorer resolution compared to F-SAR, we did this study on GEO-SAR (geosynchronous orbit high-resolution SAR) and HT-SAR (Hydroterra SAR,

scenario 4) data. We found that, as expected, long azimuth integration times deteriorate the data focusing on all parts of the image which are influenced by movement, e.g., vegetation exposed to wind, and this loss of focusing quality goes with the sensitivity to wind, i.e., depends on crop types for example. It confirms our previous studies where we noticed a defocusing on forest areas [5][6][7]. On image amplitudes or interferogram formation we found no significant impact of long azimuth integrations. The future work, with respect to this study, will be an intensive investigation of the interferogram phase and its usability for measuring the surface soil moisture (SSM). It is one of the actual goals of a future Hydroterra SAR mission.

6 Acknowledgements

This work was partially funded under ESA contract 4000134680/21/NL/FF/an.

7 Literature

[1] Hobbs, S.E., Monti-Guarnieri, A.: Geosynchronous Continental Land-Atmosphere Sensing System (G-Class): Persistent Radar Imaging for Earth Science. IEEE International Geoscience and Remote Sensing Symposium (IGARSS), 22-27 July 2018, Valencia, Spain, pp. 8621-8624

[2] Hobbs, S., Calvet, J.-C., Boni, G., Haagmans, R., Halloran, G., Hanssen, R., Kubanek, J. Mattia, F., Monti Guarnieri, A., Moreira, A., Nagler, T., Parodi, A., Lopez-Sanchez, J.M., Wadge, G., Wagner W.: Hydroterra: Exploring the Science of Rapid Water Cycle Processes Over Land ESA Living Planet Symposium, 23-27 May 2022, Bonn, Germany

[3] European Space Agency (ESA) website *ESA moves forward with Harmony*, `https://www.esa.int/Applications/Observing_the_Earth/FutureEO/Preparing_for_tomorrow/ESA_moves_forward_with_Harmony` accessed on 08 February 2024

[4] Reigber, A., et al.: Very-High-Resolution Airborne Synthetic Aperture Radar Imaging: Signal Processing and Applications, Proceedings of the IEEE 101 (3), 2012, pp. 759-783.

[5] Gracheva, V., Horn, R., Scheiber, R., Fischer, J., Keller, M., Prats, P., Reigber, A., Moreira, A.: Hydroterra's Geosynchronous Image Product Simulation using Polarimetric Airborne SAR Data, ESA Advanced RF Sensors and Remote Sensing Instruments (ARSI), 11-13 November 2019, Noordwijk, The Netherlands.

[6] Gracheva, V., Prats, P., Scheiber, R., Horn, R., Keller, M., Fischer, J., Reigber, A., Moreira, A.: Simulation of Geosynchronous Hydroterra Image Products with Airborne SAR Data, Proceedings of EUSAR, 29 March - 01 April 2021, pp. 581-586

[7] Gracheva, V., Scheiber, R., Prats, P., Horn, R., Keller, M., Fischer, Moreira, A., Kubanek, J., Haagmans, R.: Airborne SAR Experiment to Simulate Geosynchronous Hydroterra Data and Investigate the Detection of Diurnal Changes, Proceedings of IGARSS, 12-16 July 2021, pp. 3285-3288

[8] Nagler, T., Rott, H., Scheiblauer, S., Libert, L., Mölg, N., Horn, R., Fischer, J., Moreira,A., Kubanek, J.: Airborne Experiment on InSAR Snow Mass Retrieval in Alpine Environment IEEE International Geoscience and Remote Sensing Symposium (IGARSS), 17-22 July 2022, Kuala Lumpur, Malaysia

[9] Nagler, T., Rott, H., Scheiblauer, S., Mölg, N., Keuris, L., Horn, R., Fischer, J., Moreira, A., Kubanek, J.: A Field Campaign on InSAR Retrieval of Snow Mass in Alpine Terrain, 10th EARSeL Workshop on Land Ice and Snow, 06-08 February 2023, Bern, Switzerland

[10] Nagler, T., Rott, H., Scheiblauer, S., Fischer, J., Horn, R., Kubanek, J.: Experimental Studies on Dual Frequency InSAR Application for Snow Mass Monitoring, ESA FRINGE Workshop, 11-15 September 2023, Leeds, United Kingdom

[11] ESA 2020, Report for Assessment: Earth Explorer 10 Candidate Mission Hydroterra, European Space Agency, Noordwijjk, The Netherlands,ESAEOPSM-HYDRO-RP-3379, [Online]. Available: `https://esamultimedia.esa.int/docs/EarthObservation/EE10_Hydroterra_Report-for-Assessment-v1.0_13Nov2020.pdf`, accessed 08 February 2024

[12] Queiroz de Almeida, V., Matar, J., Rodriguez Cassola, M., Moreira, A., Haagmans, R., Bensi, P., Petrolati, D.: Orbit, Performance and Observation Scenarios for ESA's Earth Explorer Mission Proposal Hydroterra IEEE International Geoscience and Remote Sensing Symposium (IGARSS), 12-16 July 2021, Brussels, Belgium

[13] Prats, Pau, et al. "Distributed Imaging with TerraSAR-X and TanDEM-X." 2011 IEEE International Geoscience and Remote Sensing Symposium. IEEE, 2011. IEEE International Geoscience and Remote Sensing Symposium (IGARSS), 24-29 July 2011, Vancouver, Canada, pp. 3963-3966

[14] R. Scheiber, M. Keller, J. Fischer, C. Andreas, R. Horn, and I. Hajnsek, "Radar data processing, quality analysis and level-1b product genera- tion for AGRISAR and EAGLE campaigns," in AGRISAR and EAGLE Campaigns Final Workshop, Noordwijk, The Netherlands, Oct. 15–16, 2007

[15] Curlander, J. C., McDonough, R. N.: Synthetic Aperture Radar: Systems and Signal Pro-cessing, John Wiley, New York, 1991, p. 647

[16] Berizzi, Fabrizio, et al. "Autofocus of wide azimuth angle SAR images by contrast optimisation." IGARSS'96. 1996 International Geoscience and Remote Sensing Symposium. Vol. 2. IEEE, 1996.